International Journal of Mechanical Sciences 63 (2012) 12–25

Contents lists available at SciVerse ScienceDirect

International Journal of Mechanical Sciences

journal homepage: www.elsevier.com/locate/ijmecsci

Analytical modeling and experimental investigation of ultrasonic-vibration assisted oblique turning, part II: Dynamics analysis

H. Razavi [a], M.J. Nategh [a,*], A. Abdullah [b]

[a] Tarbiat Modares University, Mechanical Engineering Department, Tehran, P.O. Box 14115-143, Iran
[b] Amirkabir University of Technology, Mechanical Engineering Department, Tehran, Iran

ARTICLE INFO

Article history:
Received 3 January 2012
Received in revised form
6 May 2012
Accepted 11 May 2012
Available online 23 May 2012

Keywords:
Ultrasonic vibration
Vibration cutting
Oblique turning
Dynamics
Shear plane
Cutting mechanics

ABSTRACT

In the present study, a theoretical model has been developed for the analysis of the dynamics of ultrasonic-vibration assisted oblique turning. Various parameters including inclination angle, normal rake angle, tool cutting edge angle, cutting velocity, feed rate, vibration frequency and amplitude were taken into consideration in addition to other dynamics parameters such as inertial effect. The thin shear plane theory was used for the analysis. The time dependent and average cutting forces could be estimated and compared with the cutting forces in conventional turning.

1. Introduction

The oblique cutting has already been the subject of several studies [1–10]. Empirical results were needed in these studies to predict the cutting mechanics. A few theoretical models were proposed [11] that did not require experimental data to analyze the oblique cutting mechanics.

Ultrasonic vibration assisted turning (UAT) results in discontinuous machining process. Several studies [12–15] have already been carried out to assess the cutting forces in ultrasonic assisted orthogonal cutting (orthogonal UAT). The average cutting forces have been estimated in these studies by using the Fourier series or by considering the cutting forces in conventional turning (CT) multiplied by a correction factor. Studies on ultrasonic vibration assisted oblique turning (oblique UAT) are scarce. In that respect, simple analytical models [16] were proposed tackling three-dimensional cutting process to understand the fundamentals of elliptical vibration cutting at low frequencies and no dynamic effect was taken into consideration. It should be noted that the influence of feed rate has been neglected in majority of previous studies whereas it has a significant effect on the chip flow control [17,18].

In the present study, a comprehensive model has been proposed to study the cutting mechanics in oblique UAT. The tool geometry including inclination angle, normal rake angle and tool cutting edge angle and also material properties and friction have been taken into consideration in addition to other factors such as cutting speed, feed rate, vibration frequency and amplitude. It should be noted that friction has sufficiently been studied for conventional cutting, for instance in [19–23]. Some results of these studies can be employed for vibration assisted cutting. More explanation in this regard would be provided in the next part of the present study.

2. Mechanics of oblique UAT

The following parameters are involved in the study of the mechanics of oblique UAT: inclination angle i, normal rake angle γ_n, tool cutting edge angle K_r, cutting velocity V_C, feed rate V_f, vibration amplitude and frequency a, f. The thin shear plane model is assumed and thus the flow shear stress τ_s is considered to be constant on the shear plane. A sharp tool cutting edge is assumed and consequently the elastic deformation effects are neglected. The value of the average friction force angle between chip and cutting tool, β, is also considered to be constant.

The oblique cutting mechanism is schematically shown in Fig. 1. In this figure, x'' axis is collinear with the tool cutting edge, y'' axis is perpendicular to tool cutting edge in the lateral machined surface and z'' is perpendicular to tool cutting edge and also to the lateral machined surface. The important planes in oblique machining are: shear plane, tool rake face, lateral machined surface and plane normal to tool cutting edge, P_n. The latter, or actually $y''z''$ plane is taken as the reference plane in deriving the analytical relations.

It should be noted that just one part of each vibration cycle involving material removal operation has to be taken into

* Corresponding author. Tel.: +98 21 82884396.
E-mail address: nategh@modares.ac.ir (M.J. Nategh).

0020-7403/$ - see front matter © 2012 Elsevier Ltd. All rights reserved.
http://dx.doi.org/10.1016/j.ijmecsci.2012.05.005

Nomenclature

a	vibration amplitude along the cutting velocity (μm)
$\vec{a}_{ch/T}$	chip flow acceleration vector (m/s^2)
A,b',C,D,H	constants
A_S	shear plane area (mm^2)
A_o	cross section area of material entering shear zone (perpendicular to cutting velocity direction) (mm^2)
A_o^*	cross section area of material entering shear zone (perpendicular to resultant velocity direction) (mm^2)
A_*	area of shear plane cross section Projected onto a plane perpendicular to tool rake face and accommodating tool cutting edge (mm^2)
b	depth of cut (mm)
b_S	cutting edge length (mm)
$\vec{b}_S$	tool cutting edge vector (mm)
d	workpiece diameter (mm)
$\overline{D}$	rate of material flow into shear zone (mm^3/s)
$\vec{e}_{ch}$	unit vector along the chip flow direction (mm)
f	vibration frequency (Hz)
$\vec{f}_{ch}$	friction force between chip and tool rake face (N)
$\vec{f}'_{ch}$	reaction of $\vec{f}_{ch}$ (N)
$\vec{f}_S$	shear force vector on shear plane (N)
$\vec{f}'_S$	reaction of $\vec{f}_S$ (N)
h	non-deformed chip thickness (mm)
h_S	width of shear plane
h'	intermediate parameter (mm)
h'_S	width of shear plane (mm)
$\vec{h}'_S$	vector normal to cutting tool edge on shear plane (mm)
i	inclination angle (deg.)
k	number from 0 to 1
K_r	tool cutting edge angle (deg.)
L	accelerated chip length (mm)
m	chip mass (kg)
m_l	chip mass per unit length (kg/m)
$\vec{N}_{ch}$	force normal to tool rake face (N)
$\vec{N}'_{ch}$	reaction of $\vec{N}_{ch}$ (N)
$\vec{N}_S$	force normal to shear plane (N)
$\vec{N}'_S$	reaction of $\vec{N}_S$ (N)
N	spindle rotational speed (rev/min)
$\vec{n}_S$	unit vector in direction of force $\vec{f}_S$ (mm)
$\vec{n}'_S$	unit vector in shear plane and normal to $\vec{f}_S$ (mm)
P_n	plane normal to cutting edge
P_V	velocity plane
$\vec{R}_T$	resultant force applied to rake face (N)
$\vec{R}'_T$	reaction of $\vec{R}_T(N)$
$R_{T_I}(t)$	components of $\vec{R}_T(N)$; I=X, Y, Z
$\vec{R}_S(t)$	resultant cutting force applied to shear plane (N)
$\vec{R}'_S(t)$	reaction of $\vec{R}_S(t)$ (N)
t	time (s)
t_{11}	machining interruption instant in the first cycle of vibration (s)
t_{12}	instant of maximum distance of the cutting tool from the shear zone in the first vibration cycle (s)
t_{13}	machining restart instant in the first cycle of vibration (s)
t_{n1}	machining interruption instant in the nth cycle of vibration (s)
t_{n2}	instant of maximum distance of the cutting tool from the shear zone in the nth vibration cycle (s)
t_{n3}	machining restart instant in the nth cycle of vibration (s)
V	chip volume per unit length (m^3/m)
V_C	cutting speed (m/s)
$\vec{V}_{ch}$	chip flow velocity vector relative to reference configuration (m/s)
$\vec{V}_{ch/T}$	chip flow velocity vector relative to tool (m/s)
V_{cr}	critical cutting speed (m/s)
V_f	feed rate (m/s) or (mm/rev)
$\vec{V}_{S/T}$	velocity of material flow on shear plane relative to cutting tool (m/s)
$V_{X''_{W/T}}(t)$	workpiece's velocity component relative to tool in cutting tool edge direction ($x''y''z''$ coordinate system) (m/s)
$V_{Y''_{W/T}}(t)$	workpiece's velocity component relative to tool normal to cutting tool edge in lateral machined surface ($x''y''z''$ coordinate system) (m/s)
$V_{Z''_{W/T}}(t)$	workpiece's velocity component relative to tool in z'' direction (or normal to cutting tool edge and also normal to lateral machined surface ($x''y''z''$ coordinate system) (m/s)
$V_{resultant}$	resultant velocity (resultant of cutting velocity V_C and feed rate V_f) (m/s)
$\vec{V}_W$	workpiece's velocity vector in UAT (with the same magnitude as cutting speed) (m/s)
$\vec{V}_{W/T}$	workpiece's velocity vector relative to tool in UAT (m/s)
$x\ y\ z$	machine tool coordinate system: x radial (or depth of cut) direction, y tangential (or cutting velocity) direction and z axial (or negative feed) direction
$x'\ y'\ z'$	intermediate coordinate system (rotated $x\ y\ z$ system by angle $90-K_r$)
$x''\ y''\ z''$	oblique coordinate system (rotated $x'y'z'$ system by angle i); x''along the tool's cutting edge, y'' placed on the lateral surface and z''normal to the lateral surface
β	friction force angle between tool and chip (deg.)
γ_n	normal rake angle (deg.)
ε	an arbitrarily small value (deg.)
ζ	angle between resultant velocity and its y component (deg.)
η_{ch}	chip flow angle (deg.)
θ_i	angle between $\vec{R}_T$ and normal plane, P_n, (deg.)
θ'_i	angle between $\vec{R}_S$ and normal plane (deg.)
θ_n	angle between y'' axis and projection of $\vec{R}_T$ on normal plane (deg.)
$\theta_{n-CT},\theta_{i-CT},\phi_{i-CT}$	values estimated from conventional oblique cutting mechanics
θ'_n	angle between y'' axis and projection of $\vec{R}'_S$ on normal plane (deg.)
ρ	Density of workpiece material (kg/m^3)
τ_s	flow shear stress (N/mm^2)
ϕ_i	oblique shear angle (deg.)
ϕ_n	normal shear angle (measured in normal plane) (deg.)
ω	angular velocity (rad/s)

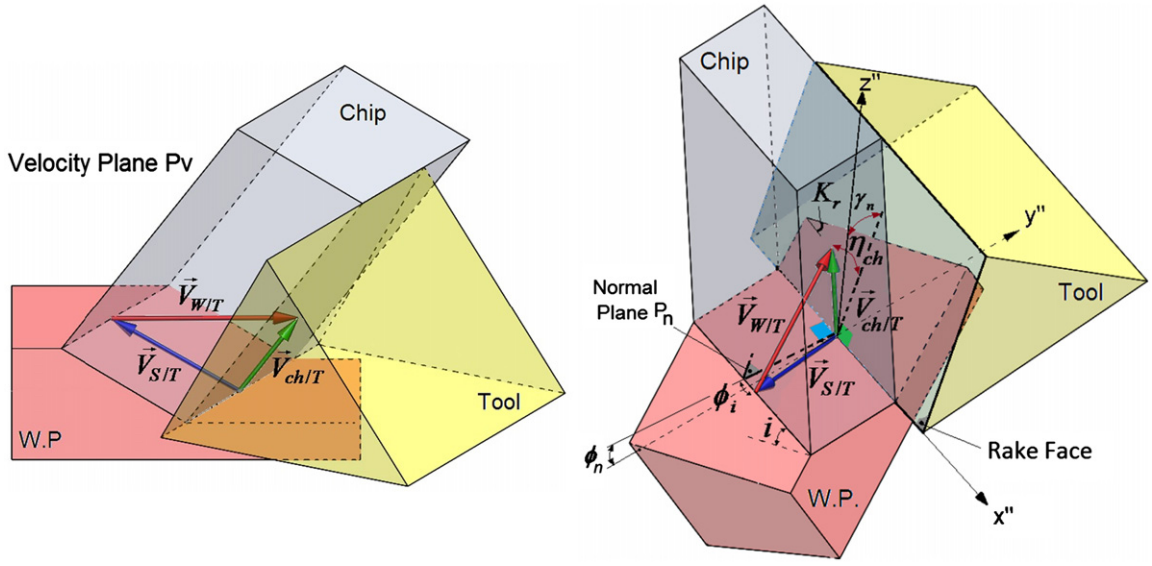

Fig. 1. Cutting mechanism in oblique machining (3D elements of the workpiece, chip and cutting tool).

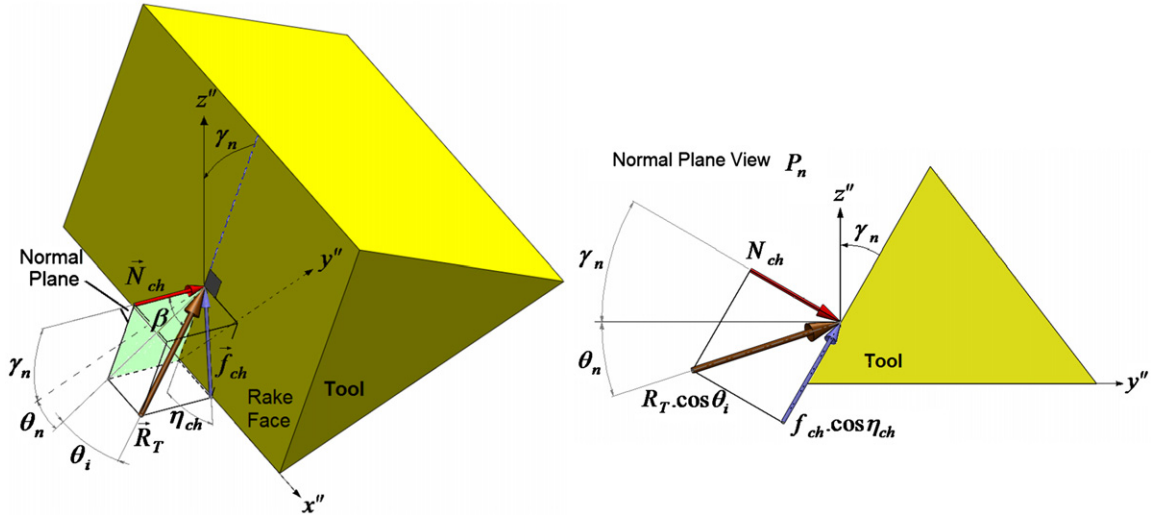

Fig. 2. Forces acting on the cutting tool rake face.

consideration and the non-cutting part need not to be analyzed. The velocity vector of chip relative to cutting tool, $\vec{V}_{ch/T}$, can be written from Fig. 1, as follows:

$$\vec{V}_{ch/T} = (V_{X'_{ch/T}}, V_{Y'_{ch/T}}, V_{Z'_{ch/T}}) = V_{ch/T}(-\sin\eta_{ch}, \cos\eta_{ch}\sin\gamma_n, \cos\eta_{ch}\cos\gamma_n) \quad (1)$$

where η_{ch} and γ_n are chip flow angle and normal rake angle, respectively. The velocity of material flow on the shear plane relative to cutting tool, $\vec{V}_{S/T}$, can be obtained as follows (Fig. 1):

$$\vec{V}_{S/T} = (V_{X'_{S/T}}, V_{Y'_{S/T}}, V_{Z'_{S/T}}) = V_{S/T}(\sin\phi_i, -\cos\phi_i\cos\phi_n, \cos\phi_i\sin\phi_n) \quad (2)$$

where φ_i and φ_n are oblique and normal shear angles, respectively. The continuity relation of velocities on the velocity plane, P_V, can be expressed as follows:

$$\vec{V}_{S/T} = \vec{V}_{ch/T} - \vec{V}_{W/T} \quad (3)$$

The workpiece's velocity relative to cutting tool can be obtained as follows [24]:

$$\vec{V}_{W/T}(t) = (V_{X'_{W/T}}(t), V_{Y'_{W/T}}(t), V_{Z'_{W/T}}(t)) = \begin{pmatrix} a\omega\sin i\sin\omega t - V_C\sin i - \cos i\cos K_r V_f, \\ -a\omega\cos i\sin\omega t + V_C\cos i - \sin i\cos K_r V_f, \\ \sin K_r V_f \end{pmatrix} \quad (4)$$

The chip flow angle, η_{ch}, can be obtained as the modified Merchant relation for oblique UAT from the above equation and Eqs. (1)–(3), as follows:

$$\tan\eta_{ch} = \frac{(V_C - a\omega\sin\omega t)[-\cos(\phi_n-\gamma_n)\sin i + \cos i\cos\gamma_n\tan\phi_i] - V_f[\cos(\phi_n-\gamma_n)A + C\cos\gamma_n\tan\phi_i]}{[-(V_C - a\omega\sin\omega t)\cos i + CV_f]\sin\phi_n} \quad (5)$$

where ω is the angular velocity and:

$$A=\frac{\sin K_r \tan \phi_i+\cos i \cos K_r \sin \phi_n}{\sin \phi_n} \tag{6}$$

$$C=\sin i \cos K_r-\frac{\sin K_r}{\sin \phi_n} \tag{7}$$

If the feed rate is to be neglected ($V_f=0$), the Merchant relation for the conventional oblique cutting [25] is achieved:

$$\tan \eta_{ch}=\frac{\tan i \cos(\phi_n-\gamma_n)-\cos \gamma_n \tan \phi_i}{\sin \phi_n} \tag{8}$$

2.1. Forces applied on the cutting tool

The forces being applied on the cutting tool rake face in oblique machining ($i\neq 0^\circ,\quad K_r\leq 90^\circ$) are shown in Fig. 2. In this figure $\vec{R}_T$ denotes the resultant force; $\vec{f}_{ch}$, the friction force between chip and tool rake; $\vec{N}_{ch}$, the force component normal to the cutting tool rake face; θ_i, the angle between $\vec{R}_T$ and normal plane P_n; and θ_n, the angle between y''axis and the projection of $\vec{R}_T$ on the normal plane. The friction force is assumed to be collinear with the direction of chip flow and make an angle, η_{ch}, with the direction perpendicular to the tool cutting edge. The angle between $\vec{N}_{ch}$ and $\vec{R}_T$ is denoted by β which is the friction angle.

The following geometric relations can be written from Fig. 2:

$$\left.\begin{aligned} f_{ch}&=R_T \sin \beta \\ f_{ch}\sin \eta_{ch}&=R_T \sin \theta_i \end{aligned}\right\} \Rightarrow \sin \theta_i=\sin \beta \sin \eta_{ch} \tag{9}$$

$$\left.\begin{aligned} f_{ch}&=N_{ch}\tan \beta \\ f_{ch}\cos \eta_{ch}&=N_{ch}\tan(\theta_n+\gamma_n) \end{aligned}\right\} \Rightarrow \tan(\theta_n+\gamma_n)=\tan \beta \cos \eta_{ch} \tag{10}$$

2.2. Forces applied to the chip

The inertial effect of chip removal process has to be taken into consideration since the relative motion between the cutting tool and workpiece in UAT is accelerated. In fact, the inertial force of chip influences the force equilibrium. The mass of chip between tool and shear plane, m, is assumed to have an acceleration of $\vec{a}_{ch/T}$. The free body diagram of chip in oblique UAT ($i\neq 0^\circ,\quad K_r\leq 90^\circ$) is shown in Fig. 3. In this figure, $\vec{R}'_T$ is the reaction of $\vec{R}_T$ acting on the face of chip which is in contact with the rake face; $\vec{f}'_{ch}$ and $\vec{N}'_{ch}$are the components of $\vec{R}'_T$ (the reaction forces of $\vec{f}_{ch}$ and $\vec{N}_{ch}$); $\vec{R}'_S$ is the reaction of $\vec{R}_S$ exerted on that face of chip which is trimmed from the shear plane; $\vec{f}'_S$ and $\vec{N}'_S$ are the components of $\vec{R}'_S$ in tangential and normal directions; $\vec{f}'_S$ is deviated from the normal plane, P_n, by the oblique shear angle ϕ_i (it is assumed here that the shear force on the shear plane is collinear with shear velocity on shear plane $\vec{V}_{S/T}$); θ'_i is the angle between the resultant force $\vec{R}'_S$and the normal plane; θ'_n is the angle between the projection of $\vec{R}'_S$ on the normal plane and y'' axis; and ϕ_n is the normal shear angle between the shear plane and y'' axis measured on the normal plane.

The force equilibrium relation for the chip can be written as follows:

$$\vec{R}'_S+\vec{R}'_T=m\vec{a}_{ch/T} \tag{11}$$

According to Fig. 3, the above equation can be decomposed as follows:

$$\begin{aligned} &R'_S(-\sin\theta'_i\hat{i}''+\cos\theta'_i\cos\theta'_n\hat{j}''+\cos\theta'_i\sin\theta'_n\hat{k}'')\\ &\quad+R'_T(+\sin\theta_i\hat{i}''-\cos\theta_i\cos\theta_n\hat{j}''-\cos\theta_i\sin\theta_n\hat{k}'')\\ &\quad=m(a_{X'_{ch/T}}\hat{i}''+a_{Y'_{ch/T}}\hat{j}''+a_{Z'_{ch/T}}\hat{k}'') \end{aligned} \tag{12}$$

In the above relation, m and $\vec{a}_{ch/T}$ should be calculated which in turn requires the shear plane area, A_S, and the volume of chip to be calculated.

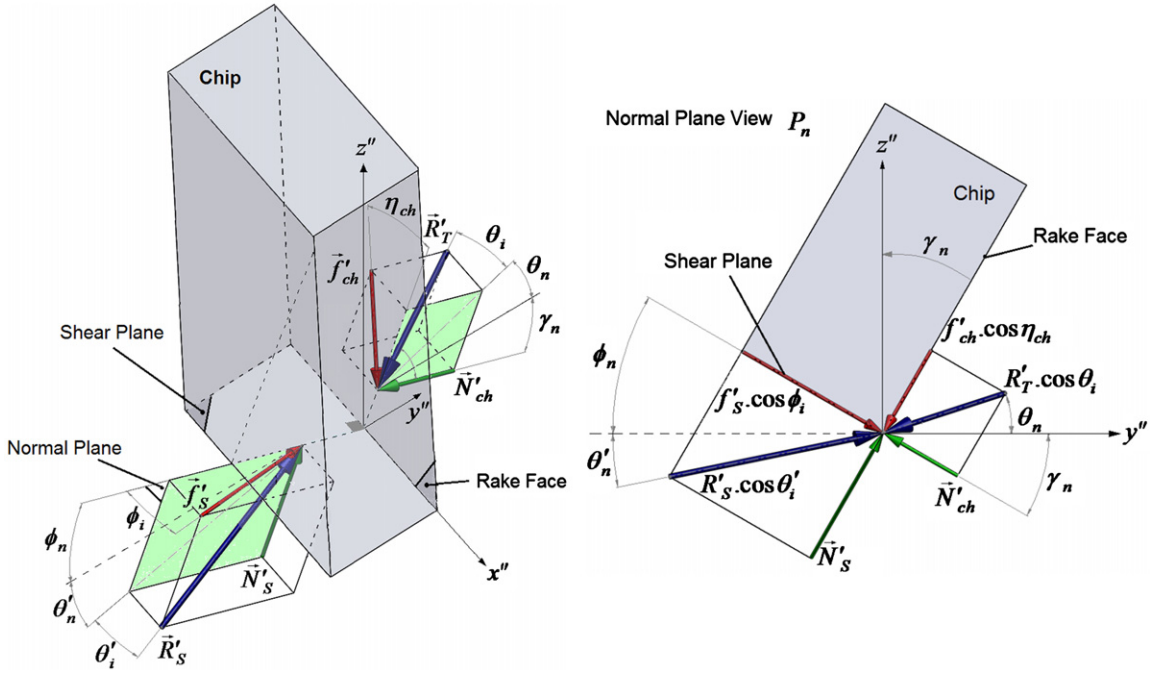

Fig. 3. Free body diagram of chip in oblique UAT.

2.2.1. Calculation of volume and mass of chip

The chip volume can be represented by three vectors $\vec{b}_S$, $\vec{h}_S$ and $\vec{e}_{ch}$ as shown in Fig. 4. The chip volume per unit length is calculated as follows:

$$V = |\vec{e}_{ch}\cdot(\vec{b}_S \times \vec{h}_S)| = |\vec{b}_S\cdot(\vec{h}_S \times \vec{e}_{ch})| = |\vec{h}_S\cdot(\vec{e}_{ch} \times \vec{b}_S)| \tag{13}$$

It is easier to calculate the chip volume in terms of $\vec{h}'_S$ than $\vec{h}_S$, so:

$$V = |\vec{e}_{ch}\cdot(\vec{b}_S \times \vec{h}'_S)| \tag{14}$$

where b_S is cutting edge length, h'_S is shear plane width and e_{ch} is unit length of chip in the chip flow direction. The vectors $\vec{b}_S$, $\vec{h}'_S$ and $\vec{e}_{ch}$ can be written as follows:

$$\vec{b}_S = b_S\hat{i}'' = \left(\frac{b'}{\cos i}\right)\hat{i}'' = \left(\frac{b/\sin K_r}{\cos i}\right)\hat{i}'' = \frac{b}{\sin k_r \cos i}\hat{i}'' \tag{15}$$

$$\vec{h}'_S = -h'_S\cos\phi_n\hat{j}'' + h'_S\sin\phi_n\hat{k}'' = -\frac{h'}{\sin\phi_n}\cos\phi_n\hat{j}'' + \frac{h'}{\sin\phi_n}\sin\phi_n\hat{k}''$$
$$= -\frac{h\sin k_r}{\sin\phi_n}\cos\phi_n\hat{j}'' + \frac{h\sin k_r}{\sin\phi_n}\sin\phi_n\hat{k}'' \tag{16}$$

$$\vec{e}_{ch} = -\sin\eta_{ch}\hat{i}'' + \cos\eta_{ch}\sin\gamma_n\hat{j}'' + \cos\eta_{ch}\cos\gamma_n\hat{k}'' \tag{17}$$

where b is depth of cut, h is the thickness of non-deformed chip which has the same value as feed rate, b' and h' are intermediate parameters. Substituting from the above equations into Eq. 13 gives:

$$V = |\vec{e}_{ch}\cdot(\vec{b}_S \times \vec{h}'_S)| = |(-\sin\eta_{ch}\hat{i}'' + \cos\eta_{ch}\sin\gamma_n\hat{j}'' + \cos\eta_{ch}\cos\gamma_n\hat{k}'')$$
$$\times\left(-\frac{bh}{\cos i}\hat{j}'' - \frac{bh\cos\phi_n}{\cos i\sin\phi_n}\hat{k}''\right)|$$
$$= \frac{bh\cos\eta_{ch}}{\cos i}\left(\sin\gamma_n + \frac{\cos\phi_n}{\sin\phi_n}\cos\gamma_n\right) \tag{18}$$

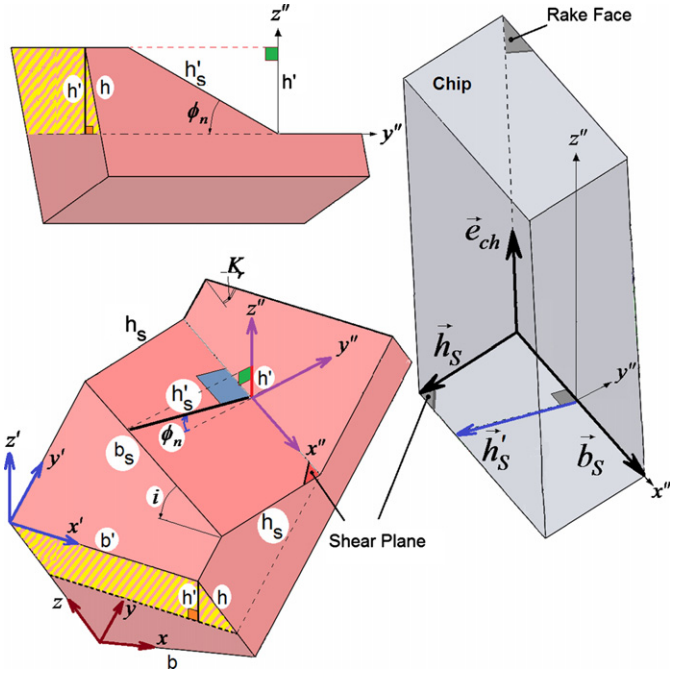

Fig. 4. Chip volume removed from the workpiece.

As a result the chip mass per unit length will be:

$$m_l = \rho V = \frac{\rho bh\cos\eta_{ch}}{\cos i}\left(\sin\gamma_n + \frac{\cos\phi_n}{\sin\phi_n}\cos\gamma_n\right) \tag{19}$$

2.2.2. Calculation of the chip acceleration

To calculate the chip acceleration, a control volume of material is considered to enter into and exit from the shear zone as shown in Fig. 5. The material is assumed to be incompressible during deformation, and thus from the mass conservation it can be written:

$$A_0 V_{W/T} = A_{ch} V_{ch/T} \tag{20}$$

where A_0 and A_{ch} are the cross section areas of the inlet and outlet material, respectively; $V_{W/T}$ is the velocity of inlet material (the workpiece's velocity relative to the cutting tool along y axis); and $V_{ch/T}$ is the velocity of the outlet material (the chip velocity relative to the cutting tool).

The velocity of the workpiece relative to the cutting tool in xyz coordinate system (regardless of feed rate $\vec{V}_f$) is $\vec{V}_{W/T} = (V_C - a\omega\sin\omega t)\hat{j}$, so the value of inlet material speed becomes $V_{W/T} = V_C - a\omega\sin\omega t$. The cross section of material before entering the shear zone (in a direction perpendicular to $\vec{V}_{W/T}$) is $A_o = bh$. The shear plane area at the inlet of shear zone is calculated, as follows:

$$A_S = \left|\vec{b}_S \times \vec{h}_S\right| = \left|\vec{b}_S \times \vec{h}'_S\right| \Rightarrow$$
$$A_S = \left|-\frac{bh}{\cos i}\hat{j}'' - \frac{bh\cos\phi_n}{\cos i\sin\phi_n}\hat{k}''\right| = \frac{bh}{\cos i}\left|\hat{j}'' + \frac{\cos\phi_n}{\sin\phi_n}\hat{k}''\right|$$
$$= \frac{bh}{\cos i}\sqrt{1 + \frac{\cos^2\phi_n}{\sin^2\phi_n}} = \frac{bh}{\cos i}\left|\frac{1}{\sin\phi_n}\right| \tag{21}$$

Since the normal shear angle ϕ_n, is in range of (0 to $\pi/2$), so the shear plane area A_S can be written as follows:

$$A_S = \frac{bh}{\cos i}\left|\frac{1}{\sin\phi_n}\right| = \frac{bh}{\cos i\sin\phi_n} \tag{22}$$

The area of the cross section of chip leaving the shear zone, A_{ch}, can be obtained by successively projecting the shear plane, first onto a plane accommodating the cutting edge and perpendicular to the rake face, then onto a plane perpendicular to both rake face and chip

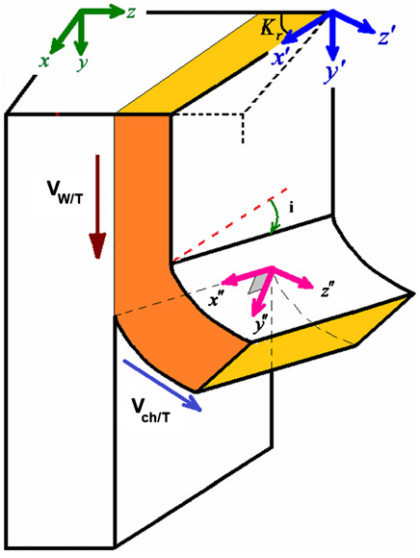

Fig. 5. Control volume of machining material.

flow direction (Fig. 6). The calculation is carried out, as follows:

$$A_* = A_S \cos(\gamma_n - \phi_n) = \frac{bh}{\cos i \sin \phi_n} \cos(\gamma_n - \phi_n) \tag{23}$$

$$A_{ch} = A_* \cos \eta_{ch} = \frac{bh}{\cos i \sin \phi_n} \cos(\gamma_n - \phi_n) \cos \eta_{ch} \tag{24}$$

where A_* is the cross section area in the first projection. The chip velocity relative to cutting tool is calculated by the aid of Eq. (19) and the above equation, as follows:

$$V_{ch/T} = \frac{A_o}{A_{ch}} V_{W/T} = \frac{\cos i \sin \phi_n}{\cos(\gamma_n - \phi_n) \cos \eta_{ch}} V_{W/T}$$
$$= \frac{\cos i \sin \phi_n}{\cos(\gamma_n - \phi_n) \cos \eta_{ch}} (V_C - a\omega \sin \omega t) \tag{25}$$

If the feed rate, V_f, is taken into consideration, the workpiece's velocity relative to the cutting tool in *xyz* coordinate system become $\vec{V}_{W/T} = (V_C - a\omega \sin \omega t)\hat{j} + V_f \hat{k}$ (Fig. 7), and:

$$V_{resultant} = \sqrt{(V_C - a\omega \sin \omega t)^2 + {V_f}^2} \tag{26}$$

$$\cos \zeta = \frac{V_C - a\omega \sin \omega t}{\sqrt{(V_C - a\omega \sin \omega t)^2 + {V_f}^2}} \tag{27}$$

where ζ is the angle between the resultant velocity and the component of workpiece's velocity relative to the cutting tool in y axis direction ($V_C - a\omega \sin \omega t$). According to Fig. 7, the area of material's cross section entering the shear zone, A_o^*, is obtained, as follows:

$$A_o^* = bh \cos \zeta = bh \frac{V_C - a\omega \sin \omega t}{\sqrt{(V_C - a\omega \sin \omega t)^2 + V_f^2}} \tag{28}$$

The rate of material flow into the shear zone, $\overline{D}$, will be:

$$\overline{D} = A_o^* V_{resultant} = bh \frac{V_C - a\omega \sin \omega t}{\sqrt{(V_C - a\omega \sin \omega t)^2 + V_f^2}} \sqrt{(V_C - a\omega \sin \omega t)^2 + V_f^2}$$
$$= bh(V_C - a\omega \sin \omega t) \tag{29}$$

It can be observed that by considering V_f, the rate of material flow into the shear zone,$\overline{D}$, does not change. By considering Eq. (19), the chip velocity relative to cutting tool can be calculated as follows:

$$V_{ch/T} = \frac{A_o^*}{A_{ch}} V_{resultant} = \frac{bh \frac{V_C - a\omega \sin \omega t}{\sqrt{(V_C - a\omega \sin \omega t)^2 + {V_f}^2}}}{\frac{bh}{\cos i \sin \phi_n} \cos(\gamma_n - \phi_n) \cos \eta_{ch}} \sqrt{(V_C - a\omega \sin \omega t)^2 + {V_f}^2}$$
$$= \frac{\cos i \sin \phi_n}{\cos(\gamma_n - \phi_n) \cos \eta_{ch}} (V_C - a\omega \sin \omega t) \tag{30}$$

The chip acceleration relative to cutting tool (in direction of chip flow) can be derived from the above equation, as follows:

$$a_{ch/T} = -\frac{\cos i \sin \phi_n \, a\omega^2 \cos \omega t}{\cos(\gamma_n - \phi_n) \cos \eta_{ch}} \tag{31}$$

The chip flow velocity can be written as $\vec{V}_{ch/T} = V_{ch/T} \vec{e}_{ch/T}$, where the unit vector along the chip flow direction, $\vec{e}_{ch/T}$, can be expressed in $x''y''z''$coordinate system by considering Eq. (1), as follows:

$$\vec{e}_{ch/T} = -\sin \eta_{ch} \hat{i}'' + \cos \eta_{ch} \sin \gamma_n \hat{j}'' + \cos \eta_{ch} \cos \gamma_n \hat{k}'' \tag{32}$$

Similarly, by considering Eq. (30) the chip flow acceleration vector in tangential direction on tool rake face can be written as follows:

$$\vec{a}_{ch/T} = -\frac{\cos i \sin \phi_n a\omega^2 \cos \omega t}{\cos(\gamma_n - \phi_n) \cos \eta_{ch}}$$
$$\times(-\sin \eta_{ch} \hat{i}'' + \cos \eta_{ch} \sin \gamma_n \hat{j}'' + \cos \eta_{ch} \cos \gamma_n \hat{k}'') \tag{33}$$

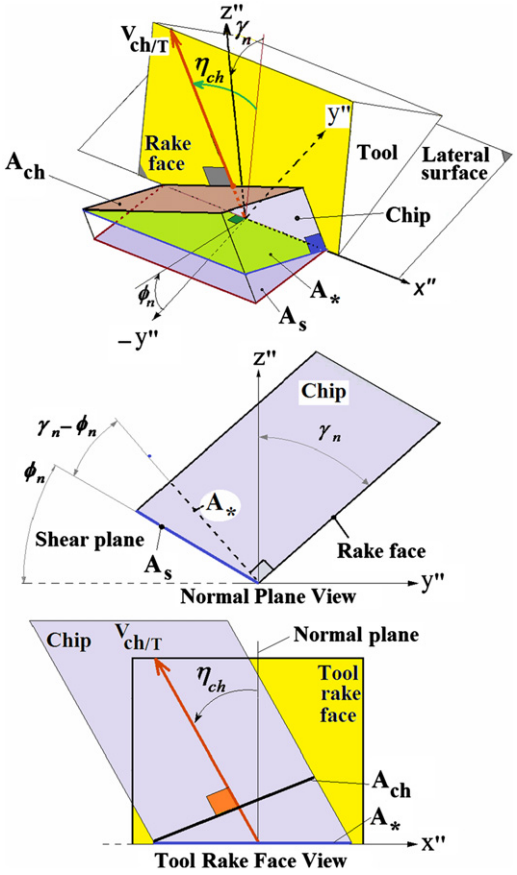

Fig. 6. Projection of shear plane.

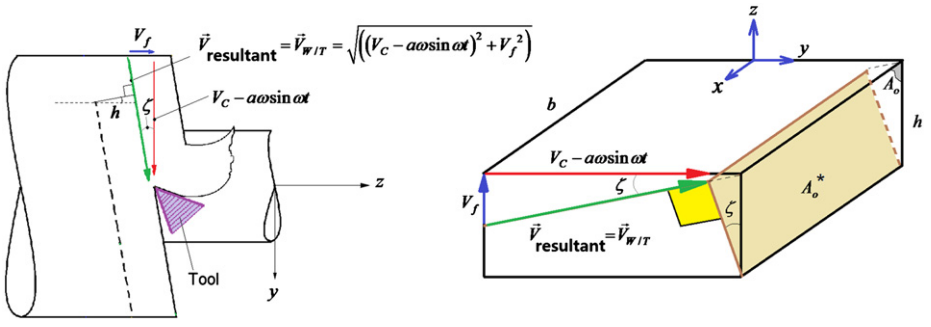

Fig. 7. Effect of feed rate on the resultant velocity and the cross section of input material.

The force equilibrium equation can now be written by substituting $\vec{a}_{ch/T}$ from the above equation into Eq. (11), as follows:

$$\begin{aligned} &R'_S(-\sin\theta'_i\hat{i''}+\cos\theta'_i\cos\theta'_n\hat{j''}+\cos\theta'_i\sin\theta'_n\hat{k''})\\ &\quad+R'_T(+\sin\theta_i\hat{i''}-\cos\theta_i\cos\theta_n\hat{j''}-\cos\theta_i\sin\theta_n\hat{k''})\\ &=m\left(-\frac{\cos i\sin\phi_n a\omega^2\cos\omega t}{\cos(\gamma_n-\phi_n)\cos\eta_{ch}}\right)\\ &\quad\times[-\sin\eta_{ch}\hat{i''}+\cos\eta_{ch}\sin\gamma_n\hat{j''}+\cos\eta_{ch}\cos\gamma_n\hat{k''}] \end{aligned} \tag{34}$$

The following equations are derived from the above equation:

$$\begin{cases} -R'_S\sin\theta'_i+R'_T\sin\theta_i=-ma_{ch/T}\sin\eta_{ch}\\ R'_S\cos\theta'_i\cos\theta'_n-R'_T\cos\theta_i\cos\theta_n=ma_{ch/T}\cos\eta_{ch}\sin\gamma_n\\ R'_S\cos\theta'_i\sin\theta'_n-R'_T\cos\theta_i\sin\theta_n=ma_{ch/T}\cos\eta_{ch}\cos\gamma_n \end{cases} \tag{35-37}$$

The mass of accelerated chip, m, is obtained from Eq. (18), as follows:

$$m=m_lL=\rho\frac{bh\cos\eta_{ch}}{\cos i}\left(\sin\gamma_n+\frac{\cos\phi_n}{\sin\phi_n}\cos\gamma_n\right)L$$

where L is the length of accelerated chip and m_l is chip mass per unit length.

In Eq. (34)–(36), the unknown parameters are L, η_{ch}, ϕ_n, θ_i, θ_n, θ'_i, θ'_n, R'_S, R'_T and t. In the present study, it is assumed that the accelerated chip length L is the same as the tool-chip contact length. The tool-chip contact length is dependent on the tool and workpiece material and also on the cutting conditions [26–28]. Astakhov obtained the contact length between 0.5 and 1.5 mm for aluminum material [28]. Grzesik suggested the contact length to be 2 times greater than seizure length and the seizure length to be equal to the uncut chip thickness [27]. Also Childs obtained the tool-chip contact length for aluminum material up to 2 mm [29]. In the present study, L is assumed to be constant and equal to 1 mm which is in acceptable range obtained by others for aluminum workpieces.

2.3. Forces applied to the shear plane

The forces acting on the shear plane in oblique turning is shown in Fig. 8. In this figure $\vec{R}_S$ is the resultant forces applied to the shear plane; $\vec{f}_S$, the tangential shear force; ϕ_i, the angle between this force and the normal plane P_n called as oblique shear angle; $\vec{N}_S$, the normal force acting on the shear plane; θ'_i, the angle between the resultant force $\vec{R}_S$ and normal plane; θ'_n, the angle between the projection of resultant force $\vec{R}_S$ on the normal plane and y'' axis; and ϕ_n, the angle between the shear plane and y''axis in the normal plane, called as normal shear angle.

The maximum shear stress theory is used to determine the angles ϕ_I and ϕ_n. In this theory it is assumed that material shearing occurs in the direction of maximum shear stress [30]. The maximum shear stress direction makes an angle of 45° with the direction of the principal stress which is the same as the direction of the resultant force $\vec{R}_S$. The angle between $\vec{f}_S$ (or $\vec{V}_{S/T}$) and $\vec{R}_S$ will, therefore, be 45° and

$$f_S=R_S[\cos\theta'_i\cos\phi_i\cos(\theta'_n+\phi_n)+\sin\theta'_i\sin\phi_i]=R_S\cos(45^\circ) \tag{38}$$

According to Fig. 8, it is clear that $\vec{n}_s\cdot\vec{n}'_s=0$ where $\vec{n}_s$ and $\vec{n}'_s$ are unit vectors in shear plane collinear with and perpendicular to $\vec{f}_S$ respectively. Since the projection of $\vec{R}_S$ to the shear plane is $\vec{f}_S$, it can be concluded that the former has no component along $\vec{n}'_s$ and thus $\vec{R}_S$ will be perpendicular to $\vec{n}'_s$. Therefore the following relation is obtained:

$$R_S[\cos\theta'_i\sin\phi_i\cos(\theta'_n+\phi_n)-\sin\theta'_i\cos\phi_i]=0 \tag{39}$$

The Eq. (39) can be simplified as follows:

$$\cos(\phi_n+\theta'_n)=\frac{\tan\theta'_i}{\tan\phi_i} \tag{40}$$

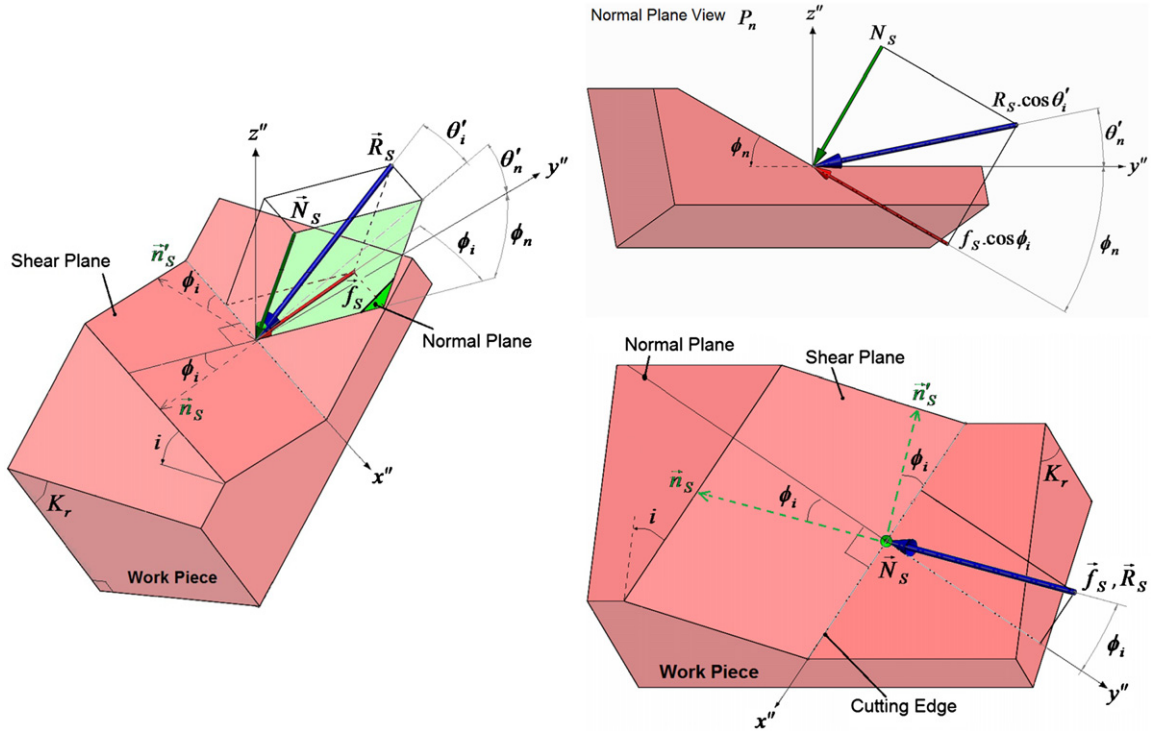

Fig. 8. Forces acting on shear plane.

By substituting Eq. (40) in Eq. (38):

$$\sin\phi_i = \sqrt{2}\sin\theta_i \tag{41}$$

In the thin shear plane theory, the shearing occurs on the shear plane, so the shear force is obtained as follows:

$$f_S = \tau_S A_S = \tau_S\left(\frac{b}{\cos i}\right)\left(\frac{h}{\sin\phi_n}\right) \tag{42}$$

By substituting f_S from the above equation into Eq. (38), the resultant forces in oblique cutting is obtained as

$$R_S = \frac{\tau_S bh}{[\cos\theta_i'\cos\phi_i\cos(\theta_n'+\phi_n)+\sin\theta_i'\sin\phi_i]\cos i\sin\phi_n} \tag{43}$$

or

$$R_S[\cos\theta_i'\cos\phi_i\cos(\theta_n'+\phi_n)+\sin\theta_i'\sin\phi_i]\cos i\sin\phi_n-\tau_S bh=0 \tag{44}$$

3. Solution of equations governing the dynamics of oblique UAT

The equations governing the dynamics of oblique UAT have already been obtained which consist of nine equations (Eqs. (5), (8), (9), (34), (35), (36), (39), (40) and (43)). A system consisting of these equations can be written as follows:

$$\begin{cases}
\tan\eta_{ch}-\frac{(V_C-a\omega\sin\omega t)[-\cos(\phi_n-\gamma_n)\sin i+\cos i\cos\gamma_n\tan\phi_i]-V_f[\cos(\phi_n-\gamma_n)A+C\cos\gamma_n\tan\phi_n]}{[-(V_C-a\omega\sin\omega t)\cos i+CV_f]\sin\phi_n}=0\\
\sin\theta_i-\sin\beta\sin\eta_{ch}=0\\
\tan(\theta_n+\gamma_n)-\tan\beta\cos\eta_{ch}=0\\
-R_S'\sin\theta_i'+R_T'\sin\theta_i=-ma_{ch/T}\sin\eta_{ch}\\
R_S'\cos\theta_i'\cos\theta_n'-R_T'\cos\theta_i\cos\theta_n=m\,a_{ch/T}\cos\eta_{ch}\sin\gamma_n\\
R_S'\cos\theta_i'\sin\theta_n'-R_T'\cos\theta_i\sin\theta_n=m\,a_{ch/T}\cos\eta_{ch}\cos\gamma_n\\
\cos(\phi_n+\theta_n')-\frac{\tan\theta_i'}{\tan\phi_i}=0\\
\sin\phi_i-\sqrt{2}\sin\theta_i'=0\\
R_S[\cos\theta_i'\cos\phi_i\cos(\theta_n'+\phi_n)+\sin\theta_i'\sin\phi_i]\cos i\sin\phi_n-\tau_S bh=0
\end{cases} \tag{45}$$

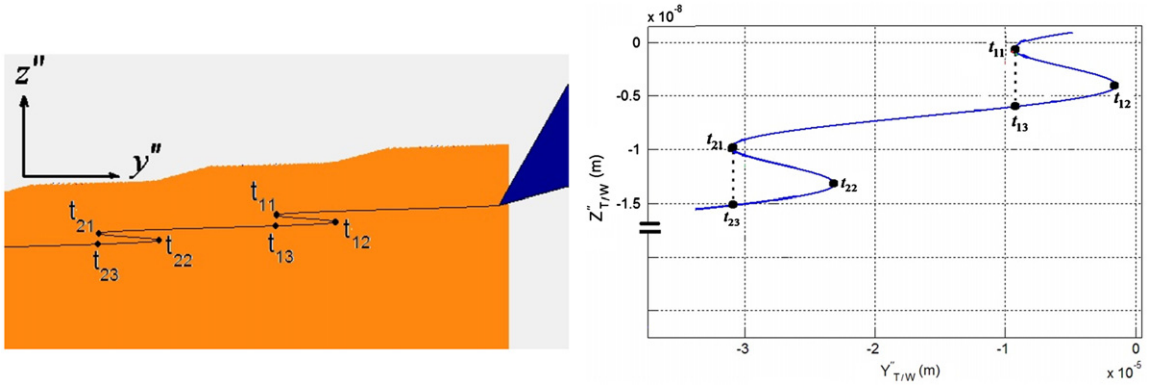

Fig. 9. Tool path relative to workpiece in oblique UAT; $i=30^\circ$, $K_r=60^\circ$, $\gamma_n=30^\circ$, $a=10$ μm, $V_f=0.2$ mm/rev, $V_C=0.53$ m/s.

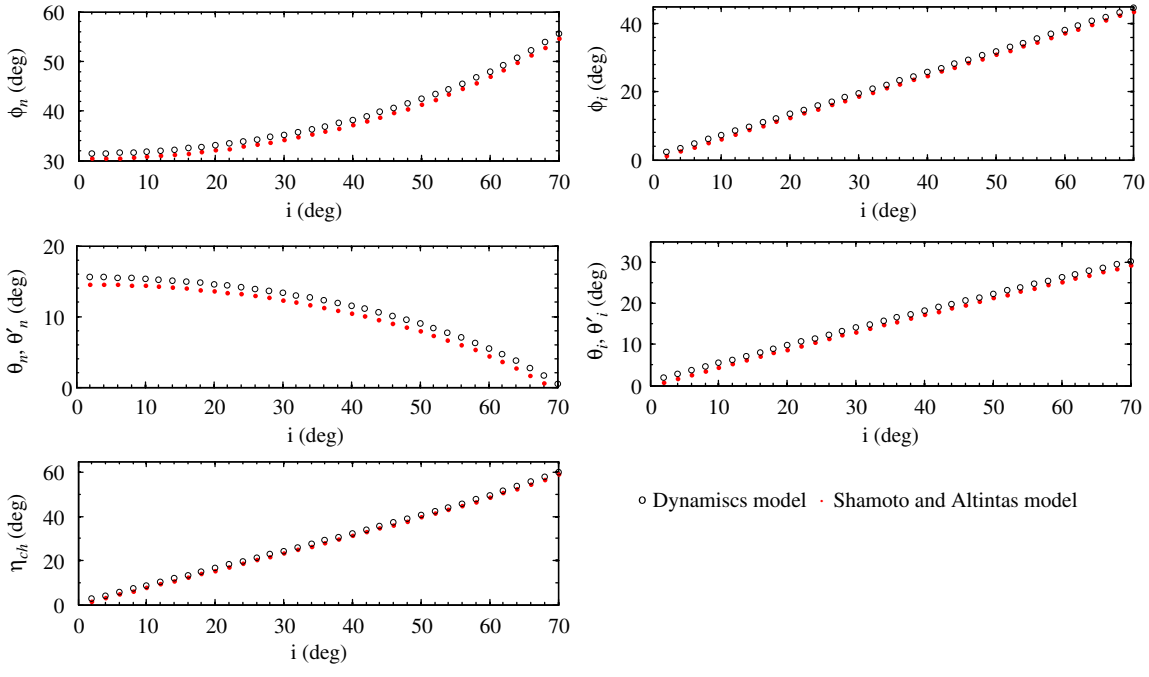

Fig. 10. Comparison of the cutting mechanics parameters in oblique CT obtained from dynamics model developed in the present study ($f=0$ or $a=0$; and $\gamma_n=20^\circ$, $K_r=90^\circ$, $V_f=0.4$ mm/rev, $\rho\cong 7800$ kg/m^3, $\tau=613$ MPa, $b=1$ mm, $L=1$ mm, $V_C=0.53$ m/s, $\beta=34.6^\circ$) with the results obtained by Shamoto and Altintas [11] ($\gamma_n=20^\circ$, $\beta=34.6^\circ$).

It should be noted that $R_T = R'_T$ and $R_S = R'_S$. The above equations should be solved for the nine unknown parameters ϕ_n, ϕ_i, θ_i, θ_n, θ'_i, θ'_n, η_{ch}, R'_S and R'_T. These equations do not have closed form solution and should be solved numerically.

The solution is obtained for that time interval of vibration cycle during which chip removal operation is done. The tool path in oblique UAT can be illustrated as in Fig. 9. The cycle time, (t_{11} to t_{21}), can be divided into two parts of non-machining (t_{11} to t_{13}) and machining (t_{13} to t_{21}) intervals. The actual chip removal operation is thus carried out during the interval,(t_{13} to t_{21}). It should be noted that the values of instants t_{11}, t_{13} and t_{21} have previously been calculated from the kinematics analysis [24]. In that study three different criteria were introduced for obtaining the above mentioned instants. It was illustrated that those criteria gave rather the same results. In the present paper, the following relations based on the first criterion are employed:

$$t_{11} = \frac{\sin^{-1}(V_C \cos i - V_f \sin i \cos K_r)/(2\pi a f \cos i)}{2\pi f} \tag{46}$$

$$t_{21} = t_{11} + 1/f \tag{47}$$

$$a \cos i \cos \omega t_{11} + V_C \cos i t_{11} - \sin i \cos K_r V_f t_{11} = a \cos i \cos \omega t_{13} + V_C \cos i t_{13} - \sin i \cos K_r V_f t_{13} \tag{48}$$

In order to solve the equations, the machining time interval, (t_{13} to t_{21}), is divided into an arbitrary number of time increment. Then for any distinct $t_k = t_{13} + k(t_{21} - t_{13})$ $(0 \le k \le 1)$, the Eq. (44) are solved and the 9 unknown parameters are obtained.

It should be noted that Eq. (44) consist of nonlinear trigonometric functions and have infinite number of solution, but only certain solutions are physically acceptable. The following boundary conditions are introduced to limit the solutions to physically acceptable ranges: the values of the resultant forces $R'_S(t)$ and $R'_T(t)$ should fall in the range of (0 to 1000) Newton; the shear plane angle is limited to ϕ_n=(0 to $\pi/2$); the chip flow angle in conventional oblique cutting is almost equal to the inclination angle, so this criterion is also adopted for oblique UAT, i.e. $\eta_{ch}(t)$=((i−ε) to (i+ε)); to find the other parameters, the solutions are bound to fall in the vicinity of the conventional oblique cutting results, as follows:ϕ_i=(($\phi_{i-CT}-\varepsilon$) to ($\phi_{i-CT}+\varepsilon$)), θ_n=(($\theta_{n-CT}-\varepsilon$) to ($\theta_{n-CT}+\varepsilon$)), $\theta'_n(t)$=(($\theta_{n-CT}-\varepsilon$) to ($\theta_{n-CT}+\varepsilon$)), θ_i=(($\theta_{i-CT}-\varepsilon$) to ($\theta_{i-CT}+\varepsilon$)) and θ'_i=(($\theta_{i-CT}-\varepsilon$) to ($\theta_{i-CT}+\varepsilon$)) where ε is a small value selected by the user. It is first assumed that ε to be$\pi/18$. Its value is changed to $\pi/15$ or $\pi/10$ if no solution is found. The Parameters θ_{n-CT}, θ_{i-CT}, ϕ_{i-CT} etc. can be estimated from the conventional oblique cutting model which is obtained from Eq. (45) by substituting the vibration frequency f=0 or amplitude a=0.

After solving for the unknown parameters, the resultant force $\vec{R}_T(t)$ obtained for $x''y''z''$ coordinate system should be transformed into forces in x y z coordinate system so that they can be measured by the dynamometer. Actually, the machining force components $\vec{R}_T(t) = (R_{T_{X''}}(t), R_{T_{Y''}}(t), R_{T_{Z''}}(t))$ are obtained by consecutive transformation of $\vec{R}_T(t)$ from $x''y''z''$ coordinates into $x'y'z'$ and then to x y z coordinates. The machining forces are obtained after these transformations, as

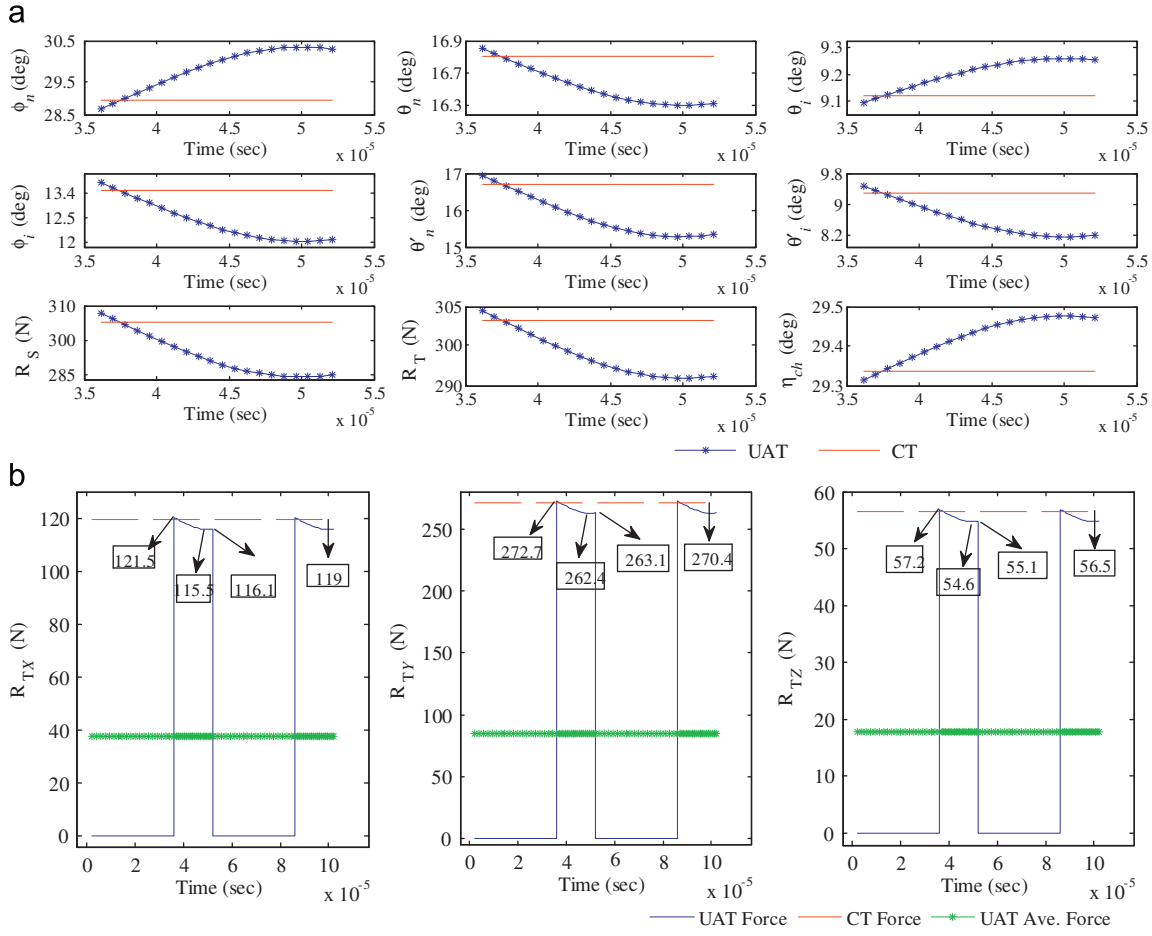

Fig. 11. Variation of (a) cutting mechanics parameters and (b) Cutting forces in oblique CT and UAT for Al2024 material, $i = 30°$, $\gamma_n = 0°$, $K_r = 75°$, f=20 kHz, a=16 μm, V_f=0.4 mm/rev, b=1 mm, L=1 mm, $V_C = 0.53$ m/s, ρ=2780 kg/m^3, τ=224 MPa, $\beta = 19°$.

follows (Appendix):

$$R_{T_X}(t) = (-\cos i \sin K_r \sin\theta_i + \sin i \sin K_r \cos\theta_i \cos\theta_n + \cos K_r \cos\theta_i \sin\theta_n) R_T(t)$$
$$R_{T_Y}(t) = (\sin i \sin\theta_i + \cos i \cos\theta_i \cos\theta_n) R_T(t)$$
$$R_{T_Z}(t) = (\cos i \cos K_r \sin\theta_i - \sin i \cos K_r \cos\theta_i \cos\theta_n + \sin K_r \cos\theta_i \sin\theta_n) R_T(t) \quad (49)$$

4. Results and discussion

In order to compare the results of the model developed in the present study with the existing models developed by others for conventional turning, the vibration frequency $f=0$ or amplitude $a=0$ is substituted in Eq. (45) to obtain CT cutting mechanics parameters. The results are compared with those obtained by Shamoto and Altintas [11] in Fig. 10. It should be noted that they have evaluated their results by comparing with the results obtained by Armarego's [31] and Lin and Oxley's [32] experimental data. Therefore, Fig. 10 actually represents a comparison between the results of the present model with the results of three other works carried out on conventional oblique cutting. It should be noted that the cutting edge angle was not considered in other works and thus $K_r = 90^\circ$ was substituted in Eq. (45). In addition, the results of other works were obtained for steel and thus $\rho \cong 7800$ kg/m^3 and $\tau = 613$ MPa [11] were used in the equations. Other conditions were similar. It can be seen from Fig. 10 that the results are closely similar.

It should be noted that no theoretical or experimental result is available for oblique UAT to be compared with the results of the present study.

The variations of different cutting mechanics parameters in oblique CT and UAT can be obtained from the foregoing theory as illustrated in Fig. 11.

It can be seen from Fig. 11a that all estimated parameters for CT remain constant while they change during the machining part of a vibration cycle in UAT. The parameters (θ_i,θ_i') and also (θ_n,θ_n') differ from each other in UAT, but are similar in CT. Also, the variations of shear angles (ϕ_n, ϕ_i) show that the cutting conditions change in UAT process. In the example presented in Fig. 11a, the difference between the estimated angles $(\phi_n, \phi_i, \theta_i, \theta_n, \theta_i', \theta_n'$ and $\eta_{ch})$ in CT and those in UAT (in machining part of the vibration cycle) is up to 2°. This is about 7 percent variation in the shear angle. The forces R_S and R_T in Fig. 11a, which are the resultant forces on shear plane and rake face respectively, show a difference about 5 N (2 percent) with each other. Each of these forces varies up to about 25 N (8 percent). This is also true for the cutting forces as the latter forces are directly obtained from R_T by using appropriate rotation matrices. In CT process, there is no difference between the forces R_S and R_T. These forces remain constant in CT.

The components of the average and the maximum UAT forces and CT forces are shown in Fig. 11b. As is clear from this figure, the average UAT forces are considerably smaller than CT forces.

As far as the cutting forces are concerned, the peak force in UAT should be taken into consideration when judging about the

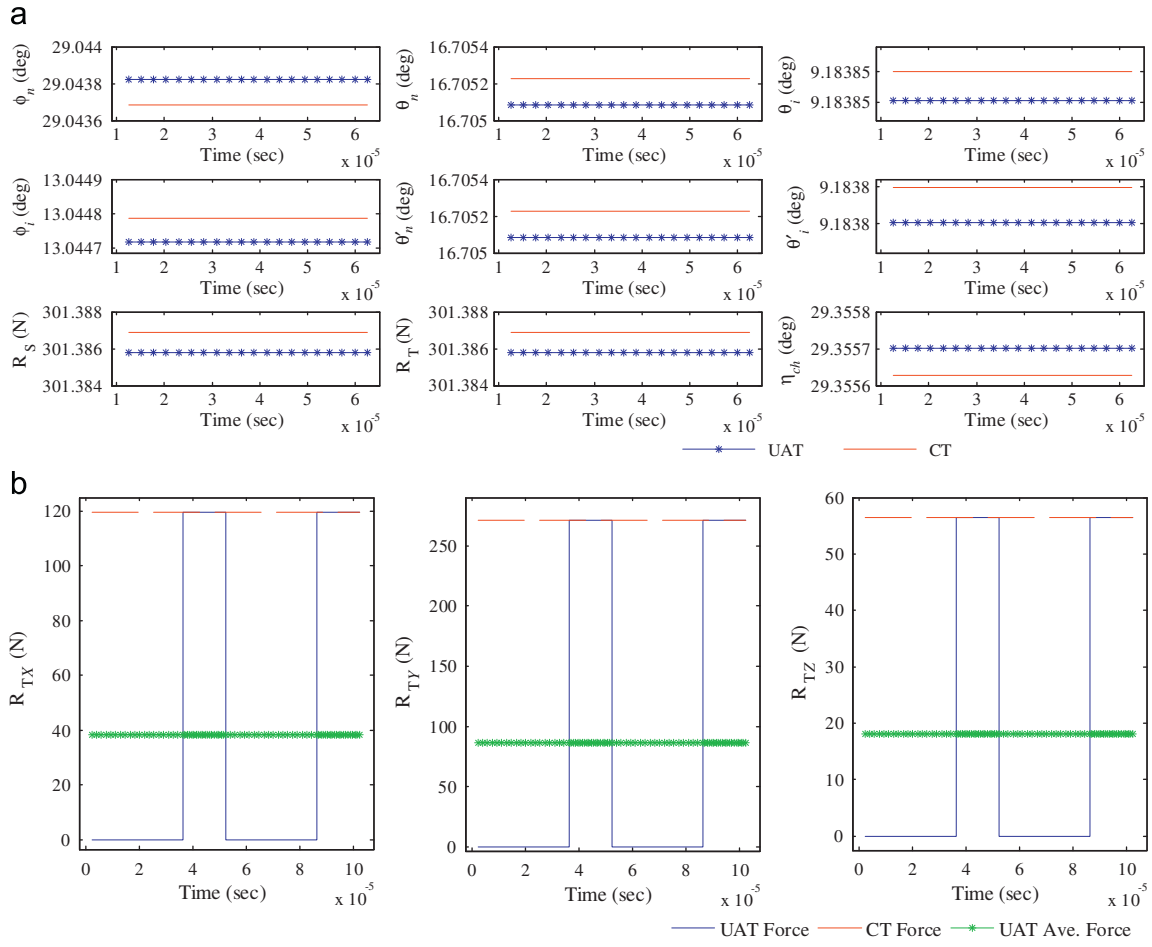

Fig. 12. Variation of (a) cutting mechanics parameters and (b) Cutting forces in oblique CT and UAT for Al2024 material in the absence of chip acceleration, $i = 30^\circ$, $\gamma_n = 0^\circ$, $K_r = 75^\circ$, $f=20$ kHz, $a=16$ μm, $V_f=0.4$ mm/rev, $b=1$ mm, $L=1$ mm, $V_C = 0.53$ m/s, $\rho=2780$ kg/m^3, $\tau=224$ MPa, $\beta = 19^\circ$ and $\vec{a}_{ch/T} = 0$.

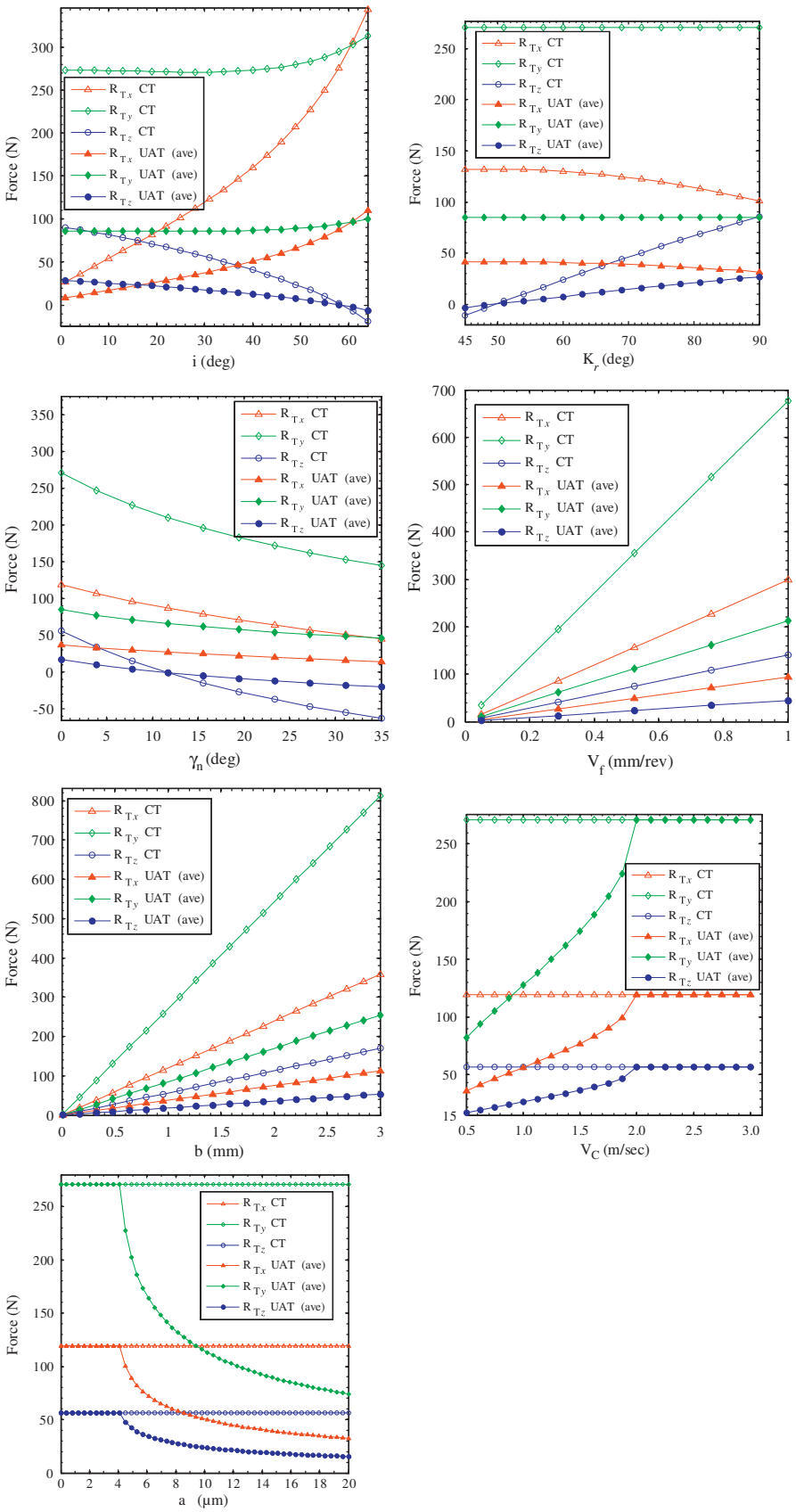

Fig. 13. Variations of cutting forces in oblique CT and UAT for Al2024 material; parameters are as follows except when they are used as the variable on the abscissa: $i=30^\circ$, $\gamma_n=0^\circ$, $K_r=75^\circ$, f=20 kHz, a=16 μm, V_f=0.4 mm/rev, b=1 mm, L=1 mm, $V_C=0.53$ m/s, ρ=2780 kg/m^3, τ=224 MPa, $\beta=19^\circ$.

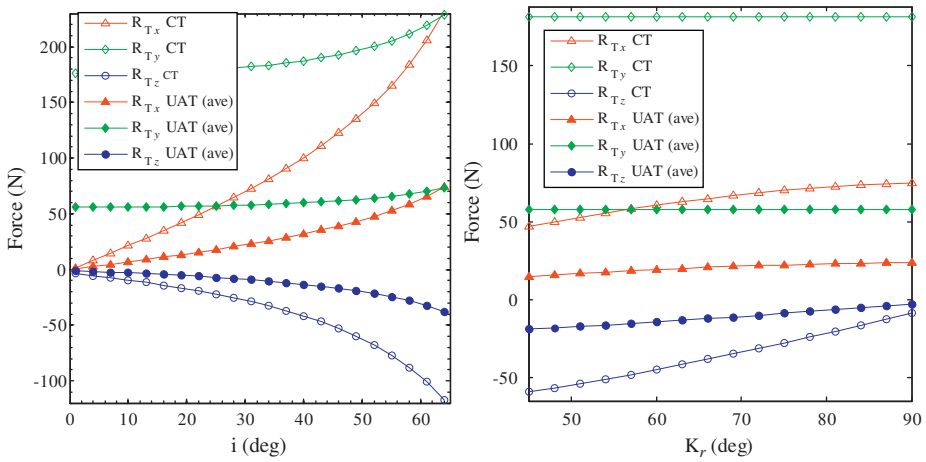

Fig. 14. Variations of cutting forces in CT and oblique UAT for Al2024 material, $\gamma_n = 20^\circ$, $i = 30^\circ$, $K_r = 75^\circ$, f=20 kHz, a=16 μm, V_f=0.4 mm/rev, b=1 mm, L=1 mm, $V_C = 0.53\ m/s$, ρ=2780 kg/m^3, τ=224 MPa, $\beta = 19^\circ$.

influence of chip acceleration; because the peak force is directly influenced by the cutting mechanism whereas the average force is dependent on the cutting and non-cutting periods in each vibration cycle. It should be noted that the average forces are considered when comparing the values of cutting forces in UAT and CT as already done in this paper. In UAT, the peak of cutting forces in the machining duration of vibration cycle is somewhat different from CT cutting forces (Fig. 11b).

The variations of cutting mechanics parameters and cutting forces in oblique UAT when the effect of chip acceleration is neglected ($\vec{a}_{ch/T} = 0$) are shown in Fig. 12. The results of oblique CT are also shown in this figure for the purpose of comparison.

It is clear from Fig. 12a that the cutting mechanics parameters do not change in the absence of the chip acceleration. The peak UAT forces and CT forces will be equal when the effect of chip acceleration is ignored (Fig. 12b). It can thus be concluded that the variations of the oblique UAT cutting mechanics parameters observed in Fig. 11 are due to the inertial effect associated with the accelerated chip produced in UAT. Additionally, the chip acceleration causes the peak UAT cutting forces to be different from CT cutting forces.

The actual material removal mechanism in UAT is influenced by the chip inertial effect. The resulting error in the estimation of the cutting mechanics parameters and cutting forces would be about 7 to 8 percent if the chip acceleration is ignored.

It is clear from Fig. 12a that the cutting mechanics parameters in UAT when obtained by ignoring the chip acceleration will be very close to their counterparts in CT with negligible differences, except for the forces. The average cutting forces in UAT are still considerably smaller in this case compared with CT in proportion of the machining duration to the total vibration cycle time (Eqs. (47) and (48)).

The variations of cutting forces in CT and oblique UAT are shown in Fig. 13 against different parameters.

In order to illustrate the effect of the normal chip angle, the cutting forces in CT and oblique UAT are obtained and shown in Fig. 14 for $\gamma_n = 20^\circ$ (instead of $\gamma_n = 0^\circ$ in Fig. 13).

It can be observed from Figs. 13 and 14 that by an increase in the inclination angle i, the radial force R_{T_X} increases; the main cutting force R_{T_Y} remains constant in the range of $i = (0$ to $45^\circ)$; and the axial force R_{T_Z} decreases in both oblique CT and UAT. These trends of change in the cutting forces have also been reported by other researcher for oblique CT [6,11,33–35].

It is also clear from Figs. 13 and 14 that by an increase in the tool cutting edge angle K_r, the main cutting force R_{T_Y} remains constant and the axial force R_{T_Z} increases in both oblique CT and UAT.

The trend of change in the radial force R_{T_X} is not so obvious; for $\gamma_n = 0^\circ$ (Fig. 13), this force shows a slight decrease with an increase in the tool cutting edge angle K_r, whereas it slightly increases for $\gamma_n = 20^\circ$ in both oblique CT and UAT.

It is also clear from Fig. 13 that by an increase in the feed rate V_f and also in the depth of cut b, the cutting forces in oblique CT and UAT increase, which is an obvious result in machining theory. By increasing the cutting velocity V_C and decreasing the vibration amplitude a, the benefits of applying ultrasonic vibration to the cutting process disappear and therefore the UAT's forces approach those in CT (Fig. 13). It can also be observed from Fig. 13 that an increase in the rake angle makes the cutting process easier due to the ensuing decrease of the cutting forces both in CT and UAT. The decrease of cutting forces at larger rake angles can also be observed by comparing the ranges of forces in Figs. 13 and 14. Smaller forces are encountered in the latter figure where the rake angle is $\gamma_n = 20^\circ$ compared with Fig. 13 where the rake angle is $\gamma_n = 0^\circ$.

It is evident from Figs. 13 and 14 that the axial cutting force becomes negative at large values of the inclination angle, tool cutting edge angle and rake angle. This is of course due to the change occurring in the direction of the resultant cutting force which in turn causes its axial component to fall along the negative z axis which is the direction of the feed motion.

5. Conclusion

A dynamics model has been developed in the present study for ultrasonic vibration assisted oblique turning (oblique UAT). The model can theoretically estimate the instantaneous cutting mechanics parameters and forces at various vibration frequencies and amplitudes and for different oblique turning parameters.

The cutting mechanics parameters and cutting forces can also be obtained for the conventional oblique turning (oblique CT) by substituting zero amplitude or zero frequency in the relevant relations developed for oblique UAT.

The average cutting forces in oblique UAT are considerably smaller than CT in all cutting conditions. The quantified evaluation of the ratio of UAT to CT cutting forces will be elaborated in part III of the present study.

The inertial effect of chip acceleration in oblique UAT is responsible for about 7 to 8 percent of change occurring in the

cutting mechanics parameters including the shear angle and the cutting forces during the machining part of the vibration cycle. Therefore, an error of about 7 to 8 percent is expected when the inertial effect is ignored. The inertial effect also causes the peak cutting forces in UAT to be somewhat different from the cutting forces in CT; whereas these forces are equal when the inertial effect is ignored.

The cutting mechanics parameters in UAT when obtained by ignoring the chip acceleration will be very close to their counterparts in CT with negligible differences, except for the forces. The average cutting forces in UAT are still considerably smaller in this case compared with CT in proportion of the machining duration to the total vibration cycle time.

By an increase in the inclination angle, the radial force increases; the main cutting force remains constant and the axial force decreases in both oblique CT and UAT.

By an increase in the tool cutting edge angle, the main cutting force remains constant and the axial force increases in both oblique CT and UAT. The trend of change in the radial force is not so obvious and is case dependent.

By increasing the feed rate and also the depth of cut, the cutting forces in oblique CT and UAT increase. By increasing the cutting speed and decreasing the vibration amplitude, the benefits of ultrasonic vibration disappear and therefore the UAT forces approach those in CT.

The cutting process is carried out easier at large rake angles due to the lower cutting forces both in CT and UAT.

Appendix A

The resultant force vector applied to the cutting tool rake face, $\overrightarrow{R}_T(t)$, in $x''y''z''$ coordinate is:

$$\overrightarrow{R}_T(t) = R_{T_{X''}}(t)\hat{i''} + R_{T_{Y''}}(t)\hat{j''} + R_{T_{Z''}}(t)\hat{k''}$$
$$R_{T_{X''}}(t) = -\sin\theta_i R_T(t)$$
$$R_{T_{Y''}}(t) = \cos\theta_i \cos\theta_n R_T(t)$$
$$R_{T_{Z''}}(t) = \cos\theta_i \sin\theta_n R_T(t) \quad (1\text{-A})$$

The $x''y''z''$ coordinates can be transformed into $x'y'z'$ coordinates, as follows:

$$\begin{bmatrix} x' \\ y' \\ z' \end{bmatrix} = \begin{bmatrix} \cos i & -\sin i & 0 \\ \sin i & \cos i & 0 \\ 0 & 0 & 1 \end{bmatrix}^{-1} \times \begin{bmatrix} x'' \\ y'' \\ z'' \end{bmatrix} = \begin{bmatrix} \cos i & \sin i & 0 \\ -\sin i & \cos i & 0 \\ 0 & 0 & 1 \end{bmatrix} \times \begin{bmatrix} x'' \\ y'' \\ z'' \end{bmatrix} \quad (2\text{-A})$$

The force components in $x''y''z''$ system can thus be converted to those in $x'y'z'$ system, as follows:

$$R_{T_{X'}}(t) = (\cos i)R_{T_{X''}}(t) + (\sin i)R_{T_{Y''}}(t) = (-\cos i \sin\theta_i + \sin i \cos\theta_i \cos\theta_n)R_T(t)$$
$$R_{T_{Y'}}(t) = (-\sin i)R_{T_{X''}}(t) + (\cos i)R_{T_{Y''}}(t) = (\sin i \sin\theta_i + \cos i \cos\theta_i \cos\theta_n)R_T(t)$$
$$R_{T_{Z'}}(t) = R_{T_{Z''}}(t) = \cos\theta_i \sin\theta_n R_T(t) \quad (3\text{-A})$$

The $x'y'z'$ coordinates can be transformed into $x\ y\ z$ coordinates, as follows:

$$\begin{bmatrix} x \\ y \\ z \end{bmatrix} = \begin{bmatrix} \cos(\pi/2-K_r) & 0 & -\sin(\pi/2-K_r) \\ 0 & 1 & 0 \\ \sin(\pi/2-K_r) & 0 & \cos(\pi/2-K_r) \end{bmatrix}^{-1} \times \begin{bmatrix} x' \\ y' \\ z' \end{bmatrix}$$
$$= \begin{bmatrix} \cos(\pi/2-K_r) & 0 & \sin(\pi/2-K_r) \\ 0 & 1 & 0 \\ -\sin(\pi/2-K_r) & 0 & \cos(\pi/2-K_r) \end{bmatrix} \times \begin{bmatrix} x' \\ y' \\ z' \end{bmatrix}$$
$$= \begin{bmatrix} \sin K_r & 0 & \cos K_r \\ 0 & 1 & 0 \\ -\cos K_r & 0 & \sin K_r \end{bmatrix} \times \begin{bmatrix} x' \\ y' \\ z' \end{bmatrix} \quad (4\text{-A})$$

The $\overrightarrow{R}_T(t)$ components in $x'y'z'$ system can thus be converted to those in $x\ y\ z$ system, as follows:

$$R_{T_X}(t) = (\sin K_r)R_{T_{X'}}(t) + (\cos K_r)R_{T_{Z'}}(t)$$
$$= (-\cos i \sin K_r \sin\theta_i + \sin i \sin K_r \cos\theta_i \cos\theta_n + \cos K_r \cos\theta_i \sin\theta_n)R_T(t)$$
$$R_{T_Y}(t) = R_{T_{Y'}}(t) = (\sin i \sin\theta_i + \cos i \cos\theta_i \cos\theta_n)R_T(t)$$
$$R_{T_Z}(t) = (-\cos K_r)R_{T_{X'}}(t) + (\sin K_r)R_{T_{Z'}}(t)$$
$$= (\cos i \cos K_r \sin\theta_i - \sin i \cos K_r \cos\theta_i \cos\theta_n + \sin K_r \cos\theta_i \sin\theta_n)R_T(t) \quad (5\text{-A})$$

References

[1] Stabler GV. The fundamental geometry of cutting tools. Proc Instn Mech Engrs 1951;165:14–21.
[2] Brown RH, Armarego EJA. Oblique machining with a single cutting edge. Int J Mach Tool Des Res 1964;4:9–25.
[3] Armarego EJA. The geometry and specification of single point lathe tools. Int J Mach Tool Des Res 1965;4:189–203.
[4] Russell JK, Brown RH. The measurement of chip flow direction. Int J Mach Tool Des Res 1966;6:129–38.
[5] Lin GCI. Prediction of cutting forces and chip geometry in oblique machining from flow stress properties and cutting conditions. Int J Mach Tool Des Res 1978;18:117–30.
[6] Lal GK. An experimental study of oblique cutting with single-edged tools. Int J Mach Tool Des Res 1982;22(No. 4):269–82.
[7] Grzesik Wit. The mechanics of continuous chip formation in oblique cutting with single-edged tool - part I: theory. Int J Mach Tool Manuf 1990;30(3):359–71.
[8] Karri V. Performance in oblique cutting using conventional methods and neural networks. Neural Comput Appl 1999;8:196–205.
[9] Becze CE, Elbestawi MA. A chip formation based analytic force model for oblique cutting. Int J Mach Tool Manuf 2002;42:529–38.
[10] Zou GP, Yellowley I, Seethaler RJ. A new approach to the modeling of oblique cutting processes. Int J Mach Tool Manuf 2009;49:701–7.
[11] Shamoto E, Altintas Y. Prediction of shear angle in oblique cutting with maximum shear stress and minimum energy principles. Trans ASME, J Manuf Sci Eng 1999;121:399–407.
[12] Kumabe Jun-ichiro. Vibration cutting—Fundamentals and applications. Jikkyo Shuppan Co. Ltd; 1979.
[13] Astashev VK, Babitsky VI. Ultrasonic cutting as a nonlinear (vibro-impact) process. Ultrasonics 1998;36:89–96.
[14] Sinn G, Zettl B, Mayer H, Stanzl-Tschegg S. Ultrasonic-assisted cutting of wood. J Mater Process Technol 2005;170:42–9.
[15] Xiaoa M, Wanga QM, Satob K, Karubeb S, Soutomeb T, Xua H. The effect of tool geometry on regenerative instability in ultrasonic vibration cutting. Int J Mach Tool Manuf 2006;46:492–9.
[16] Shamoto E, Suzuki N, Hino R. Analysis of 3D elliptical vibration cutting with thin shear plane model. CIRP Ann—Manuf Technol 2008;57:57–60.
[17] Fang N. An improved model for oblique cutting and its application to chip-control research. J Mater Process Technol 1998;79:79–85.
[18] Jwahiar IS, Luttervelt CA. Recent developments in chip control research and applications. Annals CIRP 1993;42(2):659–85.
[19] Grabec I. Chaos generated by the cutting process. Phys Lett A 1986;117: 384–6.
[20] Rusinek R, Szabelski K, Warminski J. Influence of the workpiece profile on the self-excited vibrations in a metal turning process, W:. In: Radons G, Neugebauer R, editors. Nonlinear Dynamics of Production Systems. Weinheim: Wiley-VCH; 2004. p. 153–67.
[21] Wiercigroch M, Budak E. Sources of nonlinearities, chatter generation and suppression in metal cutting. Philos Trans R Soc London, Ser A 2001;359: 663–93.
[22] Rusinek R, Szabelski K, Warminski J. Vibration analysis of two-dimensional model of metal turning process, W:. In: Cartmell MP, editor. Modern Practice in Stress and Vibration Analysis 440-441, Glasgow, IX.2003-11.IX.2003. Zurich-Uetikon: Trans Tech Publications; 2003. p. 520–6.
[23] Wiercigroch M, Krivtsov AM. Frictional chatter in orthogonal metal cutting. Philos Trans R Soc London, Ser A 2001;359:713–38.
[24] Nategh MJ, Razavi H, Abdollah A. Analytical modeling and experimental investigation of ultrasonic-vibration assisted oblique turning, part I: kinematics analysis, International Journal of Mechanical Sciences, Under Review.
[25] Merchant ME. Basic mechanics of the metal-cutting process. ASME J Appl Mech 1944;11:A168–75.
[26] Friedman MY, Lenz E. Investigation of the tool-chip contact length in metale cutting. Int J Mach Tool Des Res 1970;10:401–16.
[27] Grzesik Wit. Advanced Machining Processes of Metallic Materials: Theory, Modelling and Applications. Amsterdam: Elsevier; 2008.
[28] Astakhov Viktor P. Tribology of Metal Cutting. London: Elsevier; 2006.
[29] Childs THC, Mahdi MI, Barrow G. On the stress distribution between the chip and tool during metal turning. Annals CIRP 1989;38:55–8.

[30] Lee EH, Shaffer BW. The theory of plasticity applied to a problem of machining. ASME J Appl Mech 1951;18:405–13.
[31] Armarego EJA. Practical implications of Classical Thin Shear Zone Cutting Analyses. Singapore: UNESCO-CIRP Seminar on Manufacturing Technology; 1982.
[32] Lin GCI, Oxley PLB. Mechanics of oblique machining: predicting chip geometry and cutting forces from work material properties and cutting conditions. Proc Instn Mech Engrs 1972;186:813–20.
[33] Armarego EJA, Wiriyacosol S. Oblique machining with triangular form tools-II. Experimental investigation. Int J Mach Tool Des Res 1978;18:153–65.
[34] Venuvinod PK, Lau WS. Estimation of rake temperatures in free oblique cutting. Int J Mach Tool Des Res 1986;26(1):1–14.
[35] Kanji Ueda Keiji Manabe. Rigid-plastic F.E.M. analysis of three-dimensional deformation field in chip formation process. Annals CIRP 1993;42:35–8.